

# We are IntechOpen, the world's leading publisher of Open Access books Built by scientists, for scientists

6,900

Open access books available

186,000

International authors and editors

200M

Downloads

Our authors are among the

154

Countries delivered to

TOP 1%

most cited scientists

12.2%

Contributors from top 500 universities



WEB OF SCIENCE™

Selection of our books indexed in the Book Citation Index  
in Web of Science™ Core Collection (BKCI)

Interested in publishing with us?  
Contact [book.department@intechopen.com](mailto:book.department@intechopen.com)

Numbers displayed above are based on latest data collected.  
For more information visit [www.intechopen.com](http://www.intechopen.com)



---

# Silicon-based Integrated Microarray Biochips for Biosensing and Biodetection Applications

---

Lei Zhang, Cheng Zhu, Jinwen Geng, Xizeng Shi,  
Yunhua Gao, Zhijie Chang and He Qian

Additional information is available at the end of the chapter

<http://dx.doi.org/10.5772/60441>

---

## Abstract

The silicon-based integrated microarray biochip (IMB) is an inter-disciplinary research direction of microelectronics and biological science. It has caught the attention of both industry and academia, in applications such as deoxyribonucleic acid (DNA) and immunological detection, medical inspection and point-of-care (PoC) diagnosis, as well as food safety and environmental surveillance. Future biodetection strategies demand biochips with high sensitivity, miniaturization, integration, parallel, multi-target and even intelligence capabilities. In this chapter, a comprehensive investigation of current research on state-of-the-art silicon-based integrated microarray biochips is presented. These include the electrochemical biochip, magnetic tunnelling junction (MTJ) based biochip, giant magnetoresistance (GMR) biochip and integrated oscillator-based biochip. The principles, methodologies and challenges of the aforementioned biochips will also be discussed and compared from all aspects, e.g., sensitivity, fabrication complexity and cost, compatibility with silicon-based complementary metal-oxide-semiconductor (CMOS) technology, multi-target detection capabilities, signal processing and system integrations, etc. In this way, we discuss future silicon-based fully integrated biochips, which could be used for portable medical detection and low cost PoC diagnosis applications.

**Keywords:** Integrated microarray biochip, silicon, electrochemical, GMR, oscillator

## 1. Introduction

Silicon-based integrated microarray biochips (IMB) are an inter-disciplinary research direction of microelectronics and biological science. They have caught the attention of both industry and academia, in applications such as deoxyribonucleic acid (DNA) and immunological detection, medical inspection and point-of-care (PoC) diagnosis, as well as food safety and environmental surveillance. Future biodetection strategies demand biochips with high sensitivity, miniaturization, integration, parallel, multi-target and even intelligence capabilities [1, 2]. Recent studies focus on the high sensitivity and multi-target microarray biochips for accurate and early disease diagnosis. They also discuss treatment that is based on silicon compatible technologies due to its low cost, large-scale and readily integration with signal extraction and processing front-end and back-end circuits monolithically for a lab-on-a-chip solution [3-16]. Such studies oppose conventional assays that are currently used in hospitals and laboratories, e.g., enzyme-linked immunosorbent assay (ELISA) [17] and fluorescent detections [18], etc.

Biosensor microarray assays are one type of popular method to perform comparable biological detections. These are typically carried out for the analysis of large-scale gene and protein expression changes in a biological sample. Although there are many different forms of microarray biochips, they can be generally classified into two categories, based on the sensing methodologies: labelled and label-free. Labelled techniques tag an analyte of interest with an externally observable label such as a magnetic tag [9-16] or fluorophore [18]. On the other hand, label-free techniques detect an intrinsic property of the biomolecule such as the electrochemical charge/current [3-8], mass, thermal reactivity, etc. One typical example of label-free detection is electrochemical microarray, which senses the current induced in the binding reaction during detection. Meanwhile, magnetically labelled assays with ultra-high sensitivity, such as GMR and MTJ microarrays, are labelled techniques.

Recent studies of IMB focus on high sensitivity and multi-target microarray biochips, based on silicon compatible technologies. For example, CMOS, due to its low cost, large-scale and readily integration with signal extraction and processing front-end and back-end circuits monolithically for a lab-on-a-chip solution. State-of-the-art silicon-based IMB assays include the electrochemical microarray biochip [3-8], GMR and MTJ microarray biochips [9-14] and the fully CMOS compatible oscillator microarray biochip [15-17].

This chapter is organized as follows. Section 2 presents the electrochemical microarray biochip and illustrates examples of state-of-the-art electrochemical microarray biochips. Furthermore, design issues and considerations are elaborately analysed and discussed. Section 3 discusses magnetically labelled detection assay that are based on GMR and MTJ sensors and biochips. Methodology, trade-offs and calibration strategies are also presented, as well as a system prototype with performance evaluations and comparisons. Section 4 discusses biochip assay based on on-chip oscillator microarray that is fully compatible with modern aggressively scaled CMOS technology, with a proposed in-situ calibration strategy. Finally, the chapter concludes in Section 5, where future directions for IMB research are envisioned and reviewed.

## 2. Electrochemical microarray biochips

An electrochemical microarray biochip is one type of sensor used for DNA and protein detection. It has caught the attention of both academia and industry due to its applications in DNA and immunological analysis, analyte detection, drug delivery, trends of miniaturization and large-scale integration with CMOS technology for a system-on-a-chip (SoC) solution. In this strategy, the target detection and hybridization action are converted into electric current signals on the microarray electrodes on the chip surface. This is readily extracted by the high sensitivity analogue circuit front-end of the CMOS biochip. The integrated circuit (IC) interfacing, which is composed of an analogue circuit front-end for signal extraction, multiplexor (mux) and demultiplexor (demux) circuits for electrode enabling and decoding, as well as a potentiostat for electrode voltage stabilization, governs the overall performance of the microarray biochip.

### 2.1. Design challenges and considerations

Along with the development of micro- and nano-fabrication technologies, such as lithograph, nano-imprint, electron beam, etc., the feature size of recent electrode microarray tends to shrink towards a nanometre scale, together with the scaling down of CMOS technology. However, electrodes of nanoscale seriously suffer from background noise and random currents in a biochemical sample solution medium. This degrades the sensitivity and makes the design of IC interfacing difficult. Previous research suggests that the minimal sensitivity of signal extraction front-end IC should be at least at the order of pico-ampere (pA,  $10^{-12}$  A) or lower. Moreover, for an effective current monitoring and response, the bandwidth must be several MHz or higher - an even more difficult task. Prior applications of interfacing IC, based on potentiostat [19], trans-impedance amplifier [20] and current amplifier [21, 22] have been reported.

Large-scale integration also presents challenges regarding the signal processing back-end. For example, there are at least 20 known amino acids, while there are over 500 types of haemoglobin in human blood. A large amount of data has to be extracted and analysed by the back-end circuitry during a single detection phase. This heavily burdens the digital signal processor (DSP) or field-programmable gate array (FPGA). Recent research on neuromorphic circuits and systems, based on memristive devices and circuit, may provide a novel pathway for the large-scale, parallel signal processing and mode recognition in the near future.

The scaling down of electrode microarray is also a challenging task. Investigators have proposed a post-CMOS fabrication methodology [8]. However, when shrinking the device sizes, this methodology suffers from keyhole issues, resulting in the deterioration of the surface roughness and eventually, the sensitivity. Therefore, a co-design and fabrication regarding the microarray floor planning, lithography and etching are currently under investigation.

### 2.2. Current research

In previous studies, the electrochemical detection and sensing of DNA has been reported [3]. Here, the viability of the methodology has been verified. The first fully CMOS integrated DNA microarray biochip was published by Infineon. In this case, a 128-spot electrode structure with

in-pixel analogue-to-digital conversion was realized, achieving 100 dB of a dynamic range for direct current (DC) detection [4]. The chip was improved to a sub-nanoampere level [5] by introducing differential architecture. However, limited by the in-pixel integrator, the scale of single electrode could not be reduced beyond 100  $\mu\text{m}$ . This prevented the downscaling of the electrode feature size and the upscaling of the microarray's integration level. A fluorescent-based biosensor microarray was introduced [6], which utilized the in-pixel photo-diode. This was followed by a preamplifier and analogue-to-digital converter (ADC), which were used to detect the fluorescence on the target. A  $10^{-12}\text{A}$  level current sensitivity and a detection limit of 0.5 nM were achieved. Although a microarray is extremely sensitive in DC detection, it can hardly respond to transient signals with a bandwidth of 1 kHz and above. This is mandatory in broadband sensing (10 kHz and above) and low noise alternating current (AC) detections.

In this section, we present a fully integrated 64-pixel CMOS biosensor microarray, which is based on memory addressing architecture. Thanks to the pixel-decoding scheme, the embedded potentiostat operational amplifier (opamp) and current amplifiers are shared by all of the pixels in the microarray. This helps to reduce the pixel complexity and provides a pathway to the miniaturization of electrodes towards a nanoscale. An electrode feature size of 600 nm has been successfully demonstrated. To the best of our knowledge, this is the smallest size among published works. Moreover, the embedded current amplifier is realized with pico-ampere sensitivity in order to reconcile with the current level of the nanoscale electrodes. This is over 15 kHz bandwidth, which supports both the high-speed sensing and low noise AC detections [7, 21].

The system architecture of the proposed biosensor microarray is shown in Figure 1. It is designed with a 64-pixel of  $8 \times 8$  working electrode microarray, together with interdigital references and counter electrodes. A two-stage address decoding approach (pre-decoding and pixel-decoding) is introduced to selectively activate the microarray's working electrodes. An on-chip potentiostat opamp P is implemented to stably control the electrode potential and provide electrochemical current to the electrolyte from a negative feedback mechanism during biosensing detections. Meanwhile, an ultra-low-current amplifier (ULCA) is also integrated in order to sense the detection current and introduce amplification, before being sent out to off-chip devices. The proposed ULCA achieved a gain of 20 dB, a bandwidth of 15.5 kHz and a current sensitivity of less than 38 pA [21]. The potentiostat serving for stabilizations of electrolyte potential and accommodation of electrochemical current is realized by an opamp with a rail-to-rail input common-mode range and Class-AB output stage. The proposed biosensor microarray is realized in standard 0.18  $\mu\text{m}$  CMOS technology. Figure 2(a) shows the die micrograph of the chip, which occupies 2 mm by 2 mm of the chip area. The top electrodes of the microarray are fabricated following the procedures in previous studies [8]. Limited by the etching resolution, the minimal electrode feature size demonstrated was 600 nm, which is the smallest among published works. A biosensor detection system, based on magnetic nanoparticle (MNP), biotinlated polystyrene and streptavidin, is utilized to demonstrate the functionalities of the proposed microarray. The fluorescent results are shown in Figure 2(b) and zoomed in by Figure 2(c) and (d). The normalized fluorescent intensities are measured as 127 and 136, while the noise background is 12.3. The translating to signal-to-noise ratio (SNR)

is 10.1 dB and 10.4 dB, respectively. The measured currents start from 1~2  $\mu\text{A}$  and gradually reduce in the first 20 seconds, due to the electric shielding effect of the targets. They eventually saturate at about 20 nA and 7.3 nA, respectively.

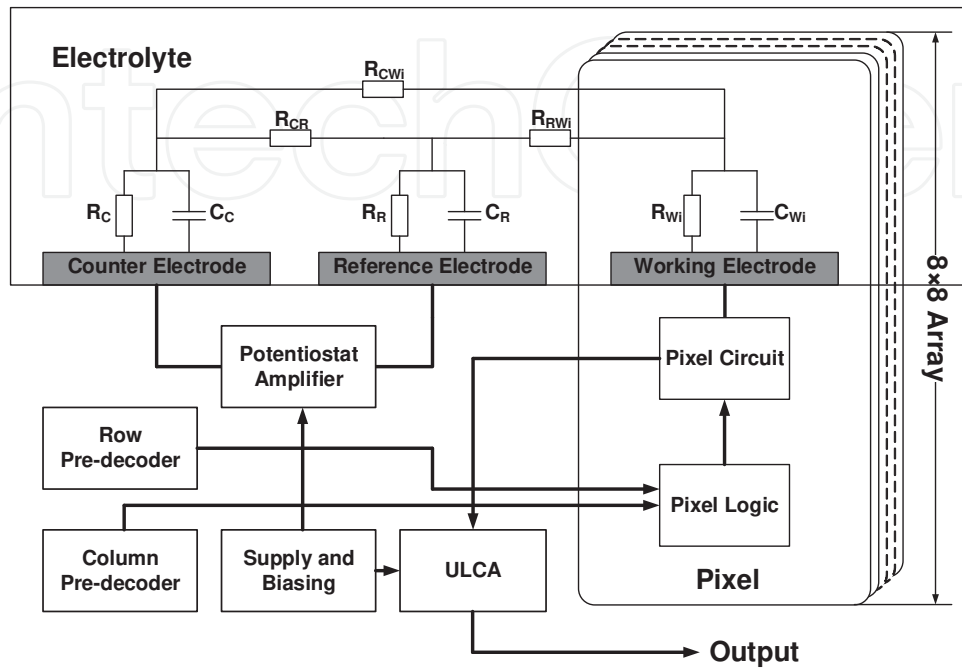


Figure 1. (a): Circuit architecture of proposed biosensor microarray.

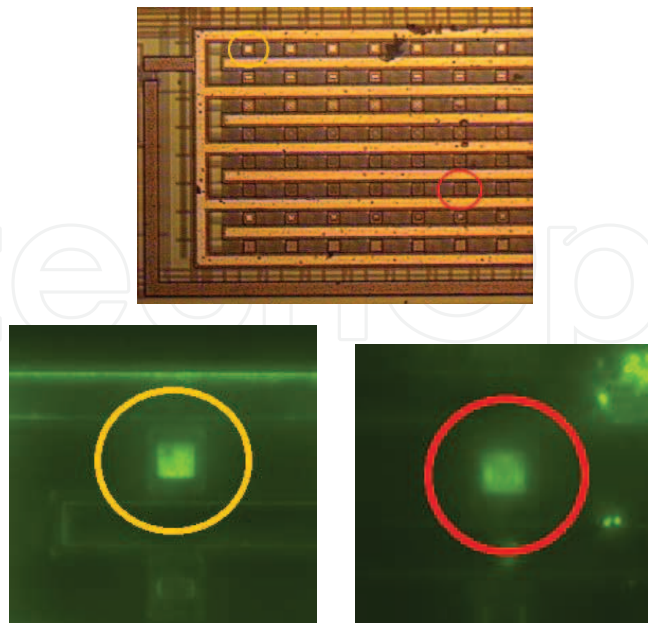


Figure 2. (a): Addressed working electrodes on the microarray, (b) fluorescent detection results on the addressed electrodes, (c) zoom in on the 8  $\mu\text{m}$  square electrode and (d) zoom in on the 600 nm spiral electrode.

### 2.3. Discussions

Electrochemical microarray biochips are one type of widely interested assay that are capable of mid-sensitivity multi-target detection. They have important applications in multi-target DNA and immunological analysis, as well as in analyte detection and drug delivery. Along with the trends of miniaturization and large-scale integration with CMOS technology for a SoC solution, various issues need to be solved in future research. Such issues include background noise and random currents in a biochemical sample solution medium during the shrinking of electrode feature size, post-CMOS fabrication technologies, parallel back-end signal processing and mode recognition. The current sensitivity of recent reported applications falls in the nano-ampere range, which is limited by background noise and random currents in the biochemical medium and buffer. This prevents its application for higher sensitivity sensing and detection applications.

## 3. GMR and MTJ microarray biochips

In recent years, rapid biological detection based on GMR and MTJ sensors and biochips is a hot issue. This is due to its interesting features such as being fast, cheap, user-friendly and acceptable high sensitivity [9-14]. As there is less magnetic material in body fluid, the magnetic signal detected by GMR and MTJ biosensors suffers minimally from the interferences of body fluid and therefore, exhibits a high sensitivity.

### 3.1. Overview

The GMR and MTJ biosensor detection system generally consists of several steps. These include the biochemical reaction on the surface of the sensor, analyte tagging by super-paramagnetic nano-particles, receiving signals from the top of the sensor, small signal extraction circuit front-end, digital domain data processing and correction back-end. These are shown in Figure 3 and Figure 4.

Figure 3 and Figure 4 show the detailed detection scheme and signal processing steps. Firstly, probe molecules that target multiple specific analytes are immobilized on the biosensor chip surface through biochemical bonding and/or reactions. During the detection phase, the analyte molecules are introduced, which are specifically captured by probes that are readily immobilized on the sensor surface. In the labelling phase, a labelling molecule tagging with MNP is subsequently bonded with analyte molecules, which are captured by probes in the detection phase. The analytes, acting as a bridge between the probe molecule and the MNP label, are therefore fixed on the surface of the biosensor chip. Finally, MNPs and analytes that are not fixed on the top of the sensor surface are washed away. The number/density of MNPs immobilized on the biosensor surface is proportional to the analyte concentration to be detected. The probe and analyte in the aforementioned detection assay can either be DNA or antigen/antibody protein, depending on the applications.

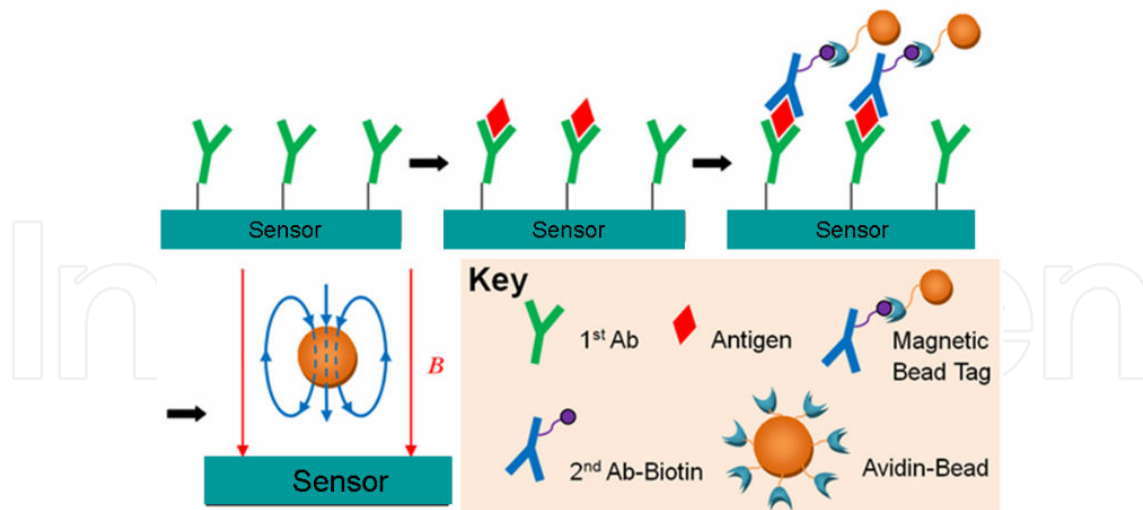


Figure 3. Biochemical detections paradigms based on MNP-labelled targets.

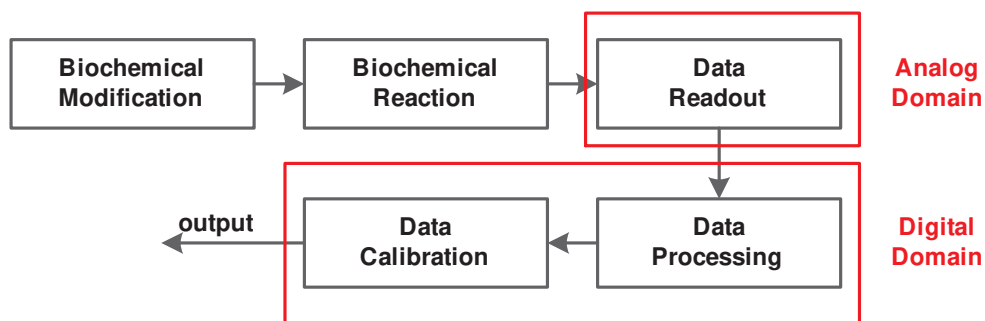


Figure 4. Signal flow and processing steps of GMR and MTJ biosensor detection system.

### 3.2. MTJ microarray biochips

Recent progress on the MTJ biosensor multi-target microarray biochip has been reported [9]. In such studies, a fully automated in vitro diagnostic (IVD) system for diagnosing acute myocardial infarction was developed. This uses high sensitivity MTJ array as sensors and 300 nm nano-magnetic particles as tags. An array of  $12 \times 10^6$  MTJ devices are integrated with a three metal layer CMOS circuit. Consequently, 48 different types of bio targets can be analysed simultaneously. A micro-fluidic cartridge, which contains all of the reagents necessary for completing the assaying process, is also assembled. Electrical, mechanical and micro-fluidic pumping devices are also integrated. The system yields results of the three major acute myocardial infarction (AMI) biomarkers (cTnI, MYO, CK-MB) in 15 minutes. An extremely high sensitivity of 0.1 ng/ml is realized and the dynamic range of detection is over three orders. However, system solutions that are based on MTJ microarray biochips are pricy in terms of the MTJ sensor itself and the circuit board/microfluidic channel integration. Meanwhile, over 100 wiring connections have to be realized and therefore lowering the yield. In the present form, this can hardly be commercialized.

### 3.3. GMR microarray biochips

GMR biosensors and biochips are proposed and utilized in the above detection assay for their acceptable high sensitivity responses to MNP labels, as well as their lower fabrication cost, compared with MTJ microarray biochips. This makes them potentially suitable for mass production and commercialization. Recent progress has been reported by researchers in Stanford [10]. In their study, 256 separate GMR sensors were fabricated and a CMOS signal extraction front-end with 16 channel  $\Sigma\Delta$  modulators was designed and realized in 180 nm CMOS process. This has a sensitivity of around 10 picomolar (pM), roughly equivalent to about 50 ppm of GMR resistance change. However, a number of issues remain unsolved. Firstly, temperature calibrations must be performed during the detection phase in order to cancel out the local temperature variation effects around the GMR sensor detection region. The calibration is made with one single fixed temperature coefficient over a wide range of GMR sensors. This incurs inaccurate results. Secondly, the biochemical buffer solution on the detection region is manually controlled on a disposable test stick. This can hardly be extended for multi-target applications with 10 or more samples and thus, is impractical with regard to efficiently controlling the biochemical reactions on multiple targets.

In this section, a complete prototype of GMR microarray biochips and system is presented. The GMR biochip, signal extraction IC, back-end signal processing, microfluidic channels, novel calibration strategies and mechanical parts with microfluidic channels are all integrated. The system performance shows a sub-50 ppm sensitivity, corresponding to roughly two 500 nm MNPs within a 1000  $\mu\text{m}^2$  GMR sensor detection area on average. This advances the present application [11].

The physical structures of the GMR biosensor are illustrated in Figure 5.

The GMR biosensor is a multilayer structure device. It has two major functionality layers: a pinned layer and a free layer. The pinned layer is a layer with fixed magnetic moment direction. Meanwhile, the free layer features a changeable magnetic moment direction, which can be modulated by an externally applied magnetic field. Both of the layers are ferromagnetic and are separated by a non-ferromagnetic layer in between them.

A GMR sensor is generally designed with two alternative structures, as shown in Figure 5. In the left subfigure, the electrons flow vertically through both the pinned and free layer (Current Perpendicular to Plane, CPP). The electrons experience scattering in ferromagnetic layers, depending on the magnetic moment of the layer and the electron spin. When the pinned and free layers exhibit parallel magnetic moment direction, the electrons experience the lowest scattering through both layers, corresponding to the lowest resistance state. If the magnetic moment directions of the pinned and free layer are antiparallel, electrons experience large scattering through both layers. This results in the highest resistance state. In the right subfigure, the electrons flow horizontally (Current In Plane, CIP). The physics of CIP is similar to the CPP structure. Furthermore, the sensor exhibits different resistances when the magnetic moment direction of the free layer is modulated by the external magnetic field. As the length of the GMR sensor is far larger than the thickness, the CPP structure normally has a higher magneto-

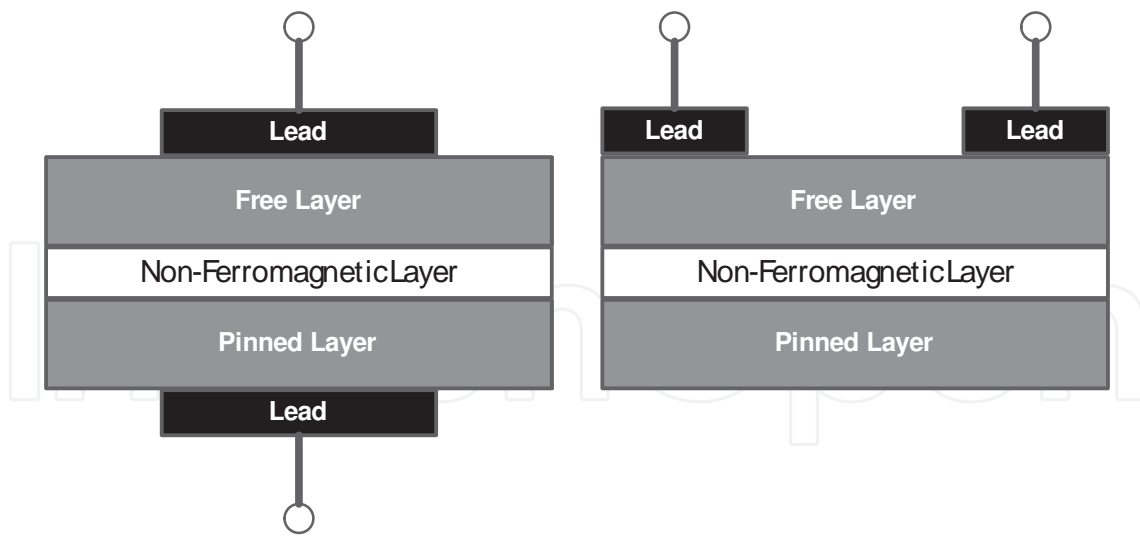


**Figure 5.** GMR biosensor structures.

resistance (MR) than its CIP counterpart. However, it is hard to fabricate and not easily integrated with the planar process. Modern GMR biosensors are generally fabricated with a CIP structure.

Super-paramagnetism MNP is utilized. This can be magnetized by the applied magnetic field and produce a small magnetic field around the MNPs, modulating the resistance of the sensor.

Firstly, a DC biasing magnetic field is applied to the sensor. This magnetic field magnetizes the MNPs on top of the sensor and forces them to produce small magnetic fields in the same direction, with the applied magnetic field on top of the sensor. An extra AC magnetic field is further applied in order to modulate the magnetic field of the MNP and consequently, induce the resistance change of the sensor itself at the same frequency.

To readout the change of the resistance of GMR sensor, a voltage is applied to the sensor. The output current flowing through the sensor is measured and readout. Considering that the flicker noise is large at a low frequency and that the resistance change caused by the MNPs is only several tens ppm of the initial resistance (chosen as a few kΩ) of the sensor, an AC voltage running at several kHz, together with an AC magnetic field at a few hundred Hz, is utilized to read out the signal. Therefore, the output current through the sensor can be calculated by the following formula:

$$I_{GMR} = \frac{V \cos(2\pi f_c t)}{R_0 + \Delta R \cos(2\pi f_s t)} = \frac{V}{R_0} \cos(2\pi f_c t) - \frac{V \Delta R}{2R_0^2} (\cos(2\pi(f_c + f_s)t) + \cos(2\pi(f_c - f_s)t)) \quad (1)$$

where  $V$  is the amplitude of the applied voltage,  $R_0$  is the initial resistance of the sensor,  $\Delta R$  is the resistance change of the sensor due to the applied magnetic field, MNPs,  $f_c$  is the frequency of the external AC voltage and  $f_s$  is the frequency of the AC magnetic field.

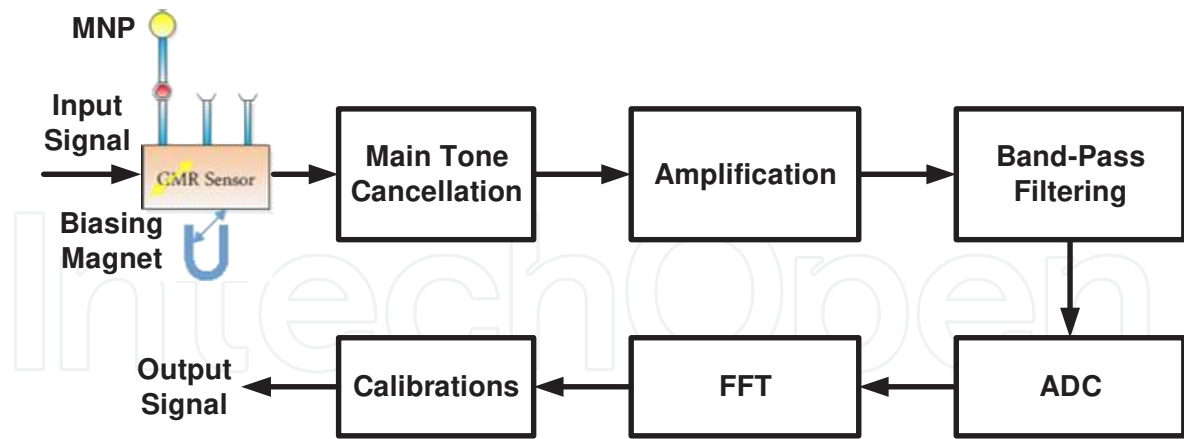


**Figure 6.** Signal processing flow of the proposed GMR sensing system, including the main tone cancellation, amplification, filtering, ADC, FFT and output correction.

It can be seen from Figure 6 that the sensor acts as a mixer and produces three tones at  $f_c$ ,  $f_c+f_s$  and  $f_c-f_s$ . As  $\Delta R$  is much smaller than  $R_0$ , the main tone amplitude at  $f_c$  is higher than the side tones amplitudes at  $f_c+f_s$  and  $f_c-f_s$ , which are signals of interest, since the effects of MNPs only relate to  $\Delta R$ .

The MR of a GMR sensor is generally less than 15%. The operation point is chosen at the middle point with maximal slope and the  $\Delta R$  is generally about 1~3% of  $R_0$ . Meanwhile, the resistance change due to MNPs can be as small as 0.1% of  $\Delta R$ . The signal is very small compared to the centre tone, requiring an ADC with a dynamic range of over 100 dB - an extremely difficult number to achieve. To overcome this issue, cancellation of the main tone is necessary. This can be implemented by applying an AC voltage with the opposite phase to a reference resistor of the same resistance as the GMR sensor. The centre tone can be reduced by at least 20 dB, considering a 10% deviation between the resistance of the GMR sensor and the cancellation resistor.

After cancellation, a filter is introduced to suppress the noise out of the band. It is followed by an amplifier before ADC in order to transform the signal from an analogue to digital domain. In the digital domain, Fast Fourier Transform (FFT) is used to calculate the frequency spectrum and eventually extract the signal from the side tones.

The signal can be extracted by the following formulas:

$$MR = \frac{4ST}{CT - 2ST} \quad (2)$$

$$\text{Signal} = \frac{MR(t) - MR(0)}{MR_{max}} \quad (3)$$

where CT is the centre tone or main tone of the GMR signal before cancellation, ST is the side tone. The centre tone amplitude before cancellation can be easily recovered based on the gain, cancelling resistance and source amplitude:

$$CT_{\text{before-cancellation}} = \frac{VR_s}{R_c} \pm CT_{\text{after-cancellation}} \quad (4)$$

with the sign decided by the resistances of the GMR sensor and the cancellation resistor.

As the sensor resistances are sensitive to the environment, output correction and calibrations of temperature variations are always necessary in order to ensure the veracity of the detection. Therefore, the temperature-calibrated scheme is proposed in this section.

Firstly, considering the temperature variations of the initial resistance of the GMR sensor and the resistance change caused by the magnetic field and MNPs, the GMR current can be written as,

$$I_{GMR} = \frac{V \cos(2\pi f_c t)}{R_0(1 + \alpha\Delta T) + \Delta R(1 + \beta\Delta T) \cos(2\pi f_s t)} \quad (5)$$

where  $\alpha$  is the temperature coefficient of the initial resistance of GMR sensor and  $\beta$  is the coefficient factor of the resistance change due to MNPs. It follows that

$$I_{GMR} \approx \frac{V}{R_0} \cos(2\pi f_c t) \left( \frac{1}{1 + \alpha\Delta T} \right) - \frac{V\Delta R}{2R_0^2} \left( \cos(2\pi(f_c + f_s)t) + \cos(2\pi(f_c - f_s)t) \right) \left( \frac{1 + \beta\Delta T}{(1 + \alpha\Delta T)^2} \right) \quad (6)$$

Then, the CT and ST can be calculated by:

$$\begin{aligned} CT(t) &= \frac{V}{R_0} \left( \frac{1}{1 + \alpha\Delta T} \right) \approx \frac{V}{R_0} (1 - \alpha\Delta T) \quad (\beta\Delta T \ll 1) \\ ST(t) &= \frac{V\Delta R}{2R_0^2} \left( \frac{1 + \beta\Delta T}{(1 + \alpha\Delta T)^2} \right) \approx \frac{V\Delta R}{2R_0^2} (1 + \beta\Delta T)(1 - 2\alpha\Delta T) \approx \frac{V\Delta R}{2R_0^2} (1 + (\beta - 2\alpha)\Delta T) \\ &\quad (\alpha\Delta T \ll 1, \beta\Delta T \ll 1) \end{aligned} \quad (7)$$

In normalizing the CT and ST to them at initial time 0, we have,

$$\begin{aligned} \frac{CT(t)}{CT(0)} &= (1 - \alpha\Delta T) \\ \frac{ST(t)}{ST(0)} &= 1 + (\beta - 2\alpha)\Delta T \end{aligned} \quad (8)$$

We can define  $\kappa$  as the following relationship between CT and ST,

$$\kappa = \frac{\left( \frac{ST(t)}{ST(0)} - 1 \right)}{\left( \frac{CT(t)}{CT(0)} - 1 \right)} = \frac{\beta - 2\alpha}{-\alpha} \quad (9)$$

One can obtain  $\kappa$  by linear fitting and utilizing the centre tone to calibrate the side tone,

$$\begin{aligned} CF &= \frac{1}{1 + \kappa \left( \frac{CT(t)}{CT(0)} - 1 \right)} = \frac{1}{1 + (\beta - 2\alpha)\Delta T} \\ ST &= ST(t) \times CF \approx \frac{V\Delta R}{2R_0^2} (1 + (\beta - 2\alpha)\Delta T) \times \frac{1}{1 + (\beta - 2\alpha)\Delta T} = \frac{V\Delta R}{2R_0^2} \end{aligned} \quad (10)$$

From the above equation, the temperature variation can be easily calibrated out during the detection. The major improvement is that the data obtained at the beginning of the test are utilized to calculate the temperature coefficient  $\kappa$  for every single sensor instead of using a standard number. Consequently, this produces a better correction and more accurately reduces the temperature effect over the whole chip.

A complete circuit and system solution prototype, including the GMR biosensor design and fabrication, small signal extraction front-end, data conversion and signal processing back-end for the GMR biosensing and detection assay, has been proposed and realized by the experiment.

The proposed GMR biosensor is a NiFe/CoFe/Cu/CoFe/PtMn multilayer structure, as shown in Figure 7(a). A 40 nm thick SiO<sub>2</sub> layer is fabricated on top of the multilayer sensor in order to keep it from oxidization and prevent electrical shorting. Furthermore, a thinner passivation layer achieves closer proximity between the magnetic particle and sensor surface for higher sensitivity, resulting in an easier electric broken down.

A biosensor chip containing 12 separate GMR sensors was fabricated, as shown in Figure 7(b). Taking into consideration the trade-off between the statistical fluctuation of magnetic particle distributions and uneven magnetic field effect during detection, the physical size of each sensor is 120  $\mu\text{m}$   $\times$  120  $\mu\text{m}$ .

In the system prototype, the signal extraction front-end with main tone cancellation, amplification and filtering functions has been realized by CMOS ICs. The sampling frequency of the ADC is 1 MHz and each packet of data contains a signal of six seconds. First, the data is divided into 60 pieces and each piece is sent to a Hanning Window for data smoothing before FFT. An average of over 10 groups of data is used to reduce the noise. An adaptive filter algorithm is

used to further reduce the noise and a 50 % noise reduction can be achieved. To further improve the sensitivity of the sensing system, the proposed temperature calibration scheme is also introduced and realized.

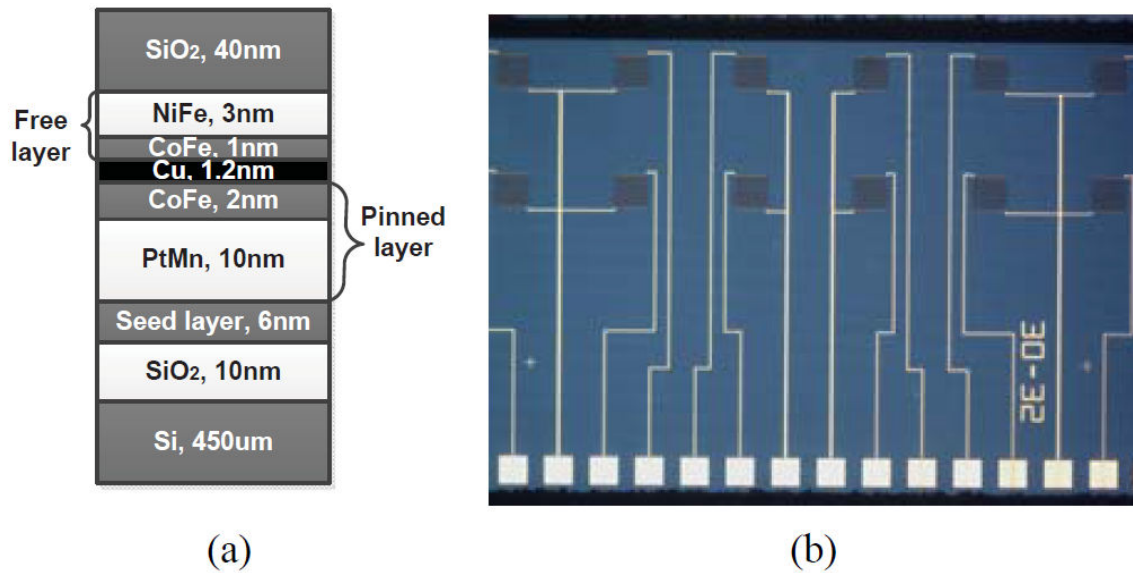


**Figure 7.** (a): Multilayer structure of the proposed GMR sensor and (b) the GMR biosensor chip containing 12 sensors.

Figure 8(a) shows the  $\alpha$  prototype detector utilizing the GMR biosensor detection scheme that is proposed in this section. The structure of the detector is shown in Figure 8(b), including the front-end circuit board, signal processing DSP, PC interface and mechanical parts of the disposable microfluidic box.

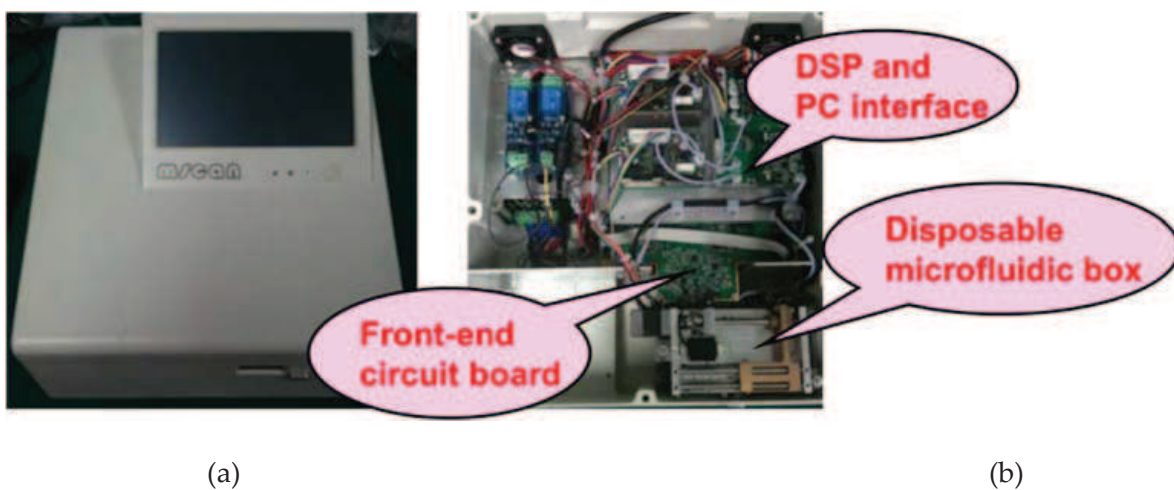


**Figure 8.** (a):  $\alpha$  prototype detector system, utilizing the proposed GMR biosensor detection scheme and microarray biochip and (b) structure of the  $\alpha$  prototype detector.

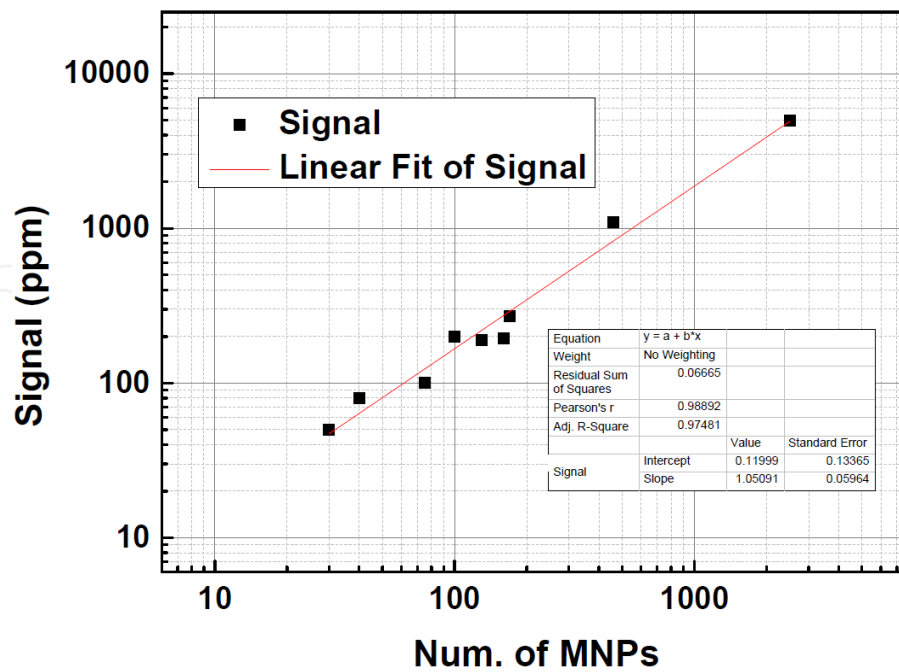


**Figure 9.** Magnetic signal versus the number of magnetic particles. Each magnetic particle produces a signal of about 2 ppm.

In the experiment, magnetic particles with diameters of 500 nm are utilized to produce the target magnetic signal. The current leakage between the two connection wires can introduce a signal as large as several hundred ppm. As a result, the data has to be collected when the surface is dry. A microscope is used to observe and count the magnetic particles on top of the sensor. The relationship between the number of magnetic particles and the output signal is shown in Figure 9. It can be seen that a sensitivity of sub-50 ppm has been achieved in the proposed system. In this case, about 30 magnetic particles on a  $120 \mu\text{m} \times 120 \mu\text{m}$  sensor surface are observed. Therefore, on average, each magnetic particle roughly produces a signal of about 2 ppm. Table 1 shows comparisons with other GMR biosensing systems. This work achieves superior performance versus prior arts. In summary, biological detections based on the proposed GMR biochips and system have been verified by experiments and a sub-50 ppm sensitivity has been reached, advancing the present work.

	Sensor Size ( $\mu\text{m} \times \mu\text{m}$ )	MNP Diameter (nm)	Min. Detectable Num. N	N per 1000 $\mu\text{m}^2$ Area
[10]	$100 \times 100$	50	2000	200
[12]	$120 \times 67.5$	30	N/A	N/A
[13]	$160 \times 58.5$	1000	N/A	N/A
[14]	1500	300	3 (theoretical)	2
This Work	$120 \times 120$	500	30	2.08

**Table 1.** Comparisons with state-of-the-art GMR biosensing systems.

### 3.4. Discussions

Magneto-sensitive detection assays are proved with extremely high sensitivities and provide full support to multi-target (~100 targets) biochemical analysis applications, e.g., DNA and immunological detections that are widely used in laboratories and hospitals. Biosensing systems and chips based on MTJ and GMR microarrays are possible candidates. Previous research suggests that a MTJ microarray biochip has a pricy sensor with unsatisfied yield. Thus, in the present form, it can hardly be commercialized. On the other hand, a GMR microarray biochip features a sub-50 ppm high sensitivity response to MNP labels and a lower fabrication cost compared to a MTJ microarray biochip. This makes it potentially suitable for mass production and commercialization in the near future. However, both biochips require an extra fabrication flow beyond the CMOS process, preventing the monolithic integration with acquisition IC front-end, signal processing back-end and DSP for a SoC solution to further improve system performance and reduce costs.

## 4. Oscillator-based microarray biochips

In the area of medical diagnosis, high accuracy, fast speed and low cost biosensor systems are always in demand. However, conventional biosensor systems, such as fluorescent labelled biosensor and MTJ and GMR biosensors, require complicated extra-process steps or fabrications. These are not fully compatible with CMOS technology and, consequently, the cost and design complexity can hardly be reduced. Moreover, both MTJ and GMR sensors require external biasing magnetic field, which complicates implementing the system.

### 4.1. Overview

An oscillator-based microarray biochip, which relies on the frequency-shift of LC oscillators, is one type of scheme that is potentially capable of solving these problems [15-17]. It uses an electromagnetic mechanism to detect the changes of output frequency, which directly corresponds to the number of targets tagged by MNPs. It potentially features high sensitivity, low cost, multi-target and easy integration, compared to GMR and MTJ biosensing strategies.

An LC oscillator is a basic component for local oscillation (LO) generation in radio-frequency (RF) integrated circuits [23]. An inductor and a fixed capacitor oscillate at a free running frequency  $f_0$ , driven by a negative resistance from a cross-coupled transistor pair. We suppose that some probe molecules are deposited on the inductor surface. During the detection phase, some target molecules with MNPs labels are also deposited on the inductor and bonded with the probes. Therefore, the MNPs change the magnetic field around the detection region defined by the inductor, effectively changing the inductance  $L_0$  to  $L_0 + \Delta L$ . This eventually shifts the oscillation frequency  $f_0$ , as shown in Eq. (11), where  $M$  is the target concentration and  $\alpha$  is a factor.

$$f = \frac{1}{2\pi\sqrt{(L_0 + \Delta L)C}} \approx f_0 \left(1 - \frac{\Delta L}{2L_0}\right) = f_0 \left(1 - \frac{\alpha M}{2L_0}\right) \quad (11)$$

The frequency shift  $\Delta f$  is proportional to the inductance change  $\Delta L$  and therefore, reflects the target molecule concentration in a sample solution.

The principle of the oscillator-based high sensitivity multi-target biochip detection is illustrated in Figure 10. Firstly, the CMOS biochip surface with multiple detection regions is treated by various probe molecules, which are a target of interest for probe immobilization, as shown in Figure 10(a) and (b). During the detection phase, the sample solutions with target molecules labelled with MNPs are brought to the detection region by either droplet or microfluidic channel for chemical bonding and hybridization. The chip is then rinsed by DI water for surface cleaning in order to remove non-specific bonding or contaminations. Eventually, the electric signal induced by the tag MNPs on the target of interest is detected by the buried CMOS signal extraction front-end circuit and conveyed off-chip (or to the on-chip ASIC) for signal processing by the back-end circuits. Since the chemical bonding and hybridization between the probe and target are specific, multiple target detections from one sample droplet can, therefore, be realized in parallel on the single biochip. This increases the detection efficiency and reduces the cost. Depending on the non-specific bonding rate between the different probes and targets, the number of targets supported by a single detection has to be traded with the fake positive rate and detection sensitivity.

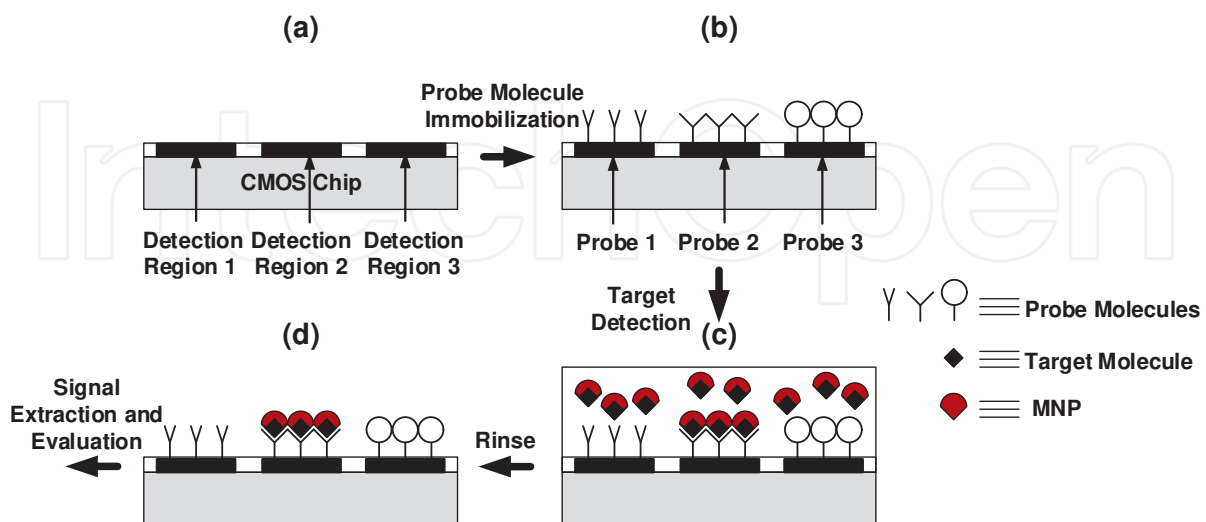


Figure 10. Oscillator-based high sensitivity multi-target biochip detection sketch.

## 4.2. Design challenges and considerations

### 4.2.1. Sensor design

#### 4.2.1.1. Running frequency

The free running frequency  $f_0$  of the oscillator has to be optimized, based on the considerations of phase noise, inductor detection region geometry and the response frequency of MNPs. Most MNPs with a diameter of 500 nm or below exhibit a response frequency of lower than 1.5 GHz [24], defining the upper boundary of  $f_0$ . Although a low  $f_0$  would present a lower phase noise, other factors include increasing the number of turns of the inductor itself, shrinking the effective detection region size and degrading the uniformity of magnetic field on the surface. Among the above factors, experiments suggest an  $f_0$  of around 1 GHz - 1.5 GHz, with a proper trade-off.

#### 4.2.1.2. $Q$ of the inductor

The quality factor ( $Q$ ) of the inductor also has to be optimized, considering the sensor dimension and phase noise of the LO oscillator, which directly correlate to the sensitivity of the biochip. Sensor dimensions are normally established from the chip size, multi-target capabilities and microfluidic channel structures, etc. For a given sensor size, the  $Q$  of the inductor can be improved by optimizing the number of metal layers, turns, trace width and spacing of the traces. For example, in a standard 180 nm CMOS process, the  $Q$  of the inductor can be maximized as 5.2 by paralleling the top three to four layers of metals with a reasonable inductance of 1.7 nH in a chip area of  $130 \mu\text{m} \times 130 \mu\text{m}$ . This is a fairly desirable value in the design, as shown in Figure 11.

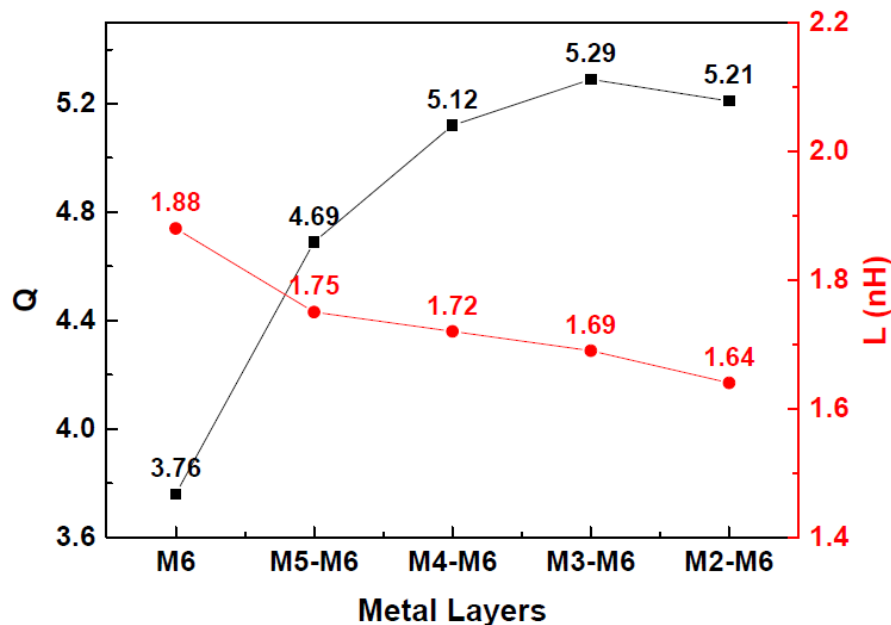


Figure 11.  $Q$  and inductance of an optimized inductor versus metal layers.

#### 4.2.1.3. Uniformity of the magnetic field

Uniformity of the surface magnetic field becomes important when the sensitivity is pushed aggressively to an extremely low level or even for single molecule/MNP detection applications. In this case, it has to be co-optimized with  $Q$  and the inductance of the inductor itself. Bowl-shape [16] and multi-layer structured [25] round shape inductor sensors are investigated to improve the field uniformity. However, the  $Q$  of the inductor of interest is substantially degraded. A non-uniform inductor trace width strategy has been investigated to improve the field uniformity. For example, as the trace width of the inner winding has been adjusted to  $9\ \mu\text{m}$ , as opposed to a width of  $8\ \mu\text{m}$ , for the rest of the outer windings in a three turn inductor, the field uniformity can be decently improved, as shown in Figure 12. It can be seen that the magnetic field intensity varies by roughly 20 % over the inductor surface before optimization. With the proposed technique, it is reduced to about 5 %.

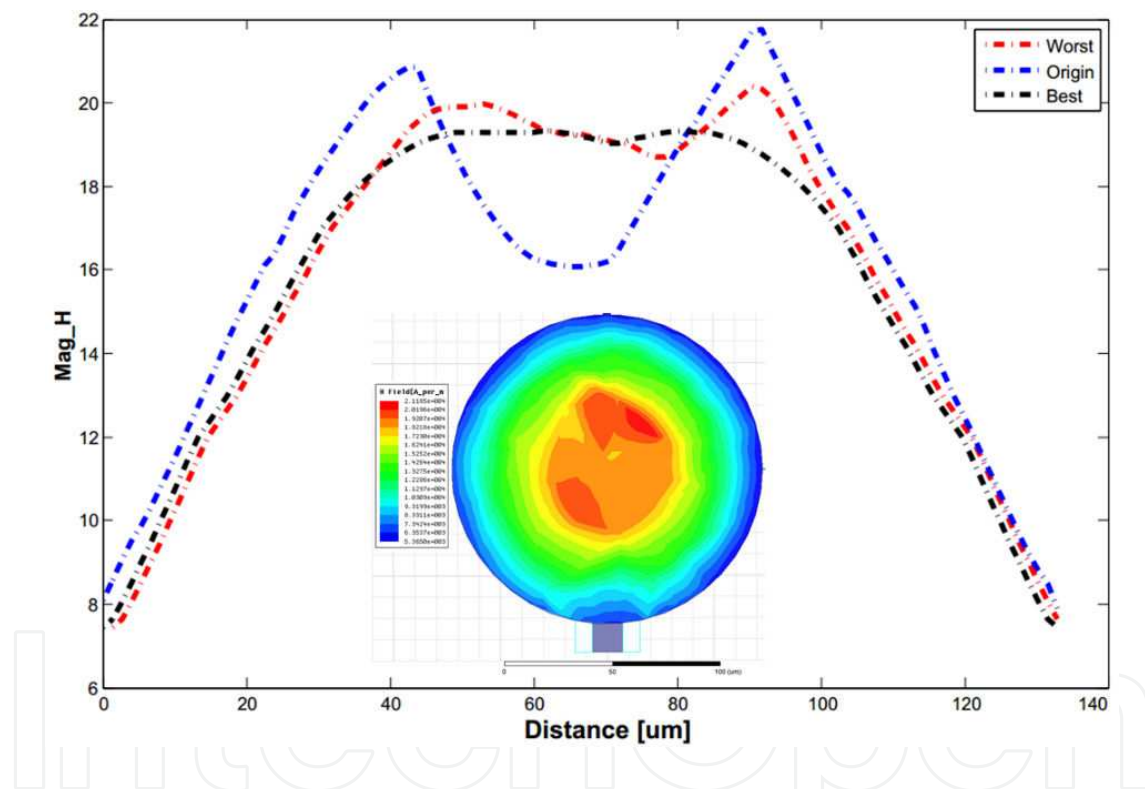
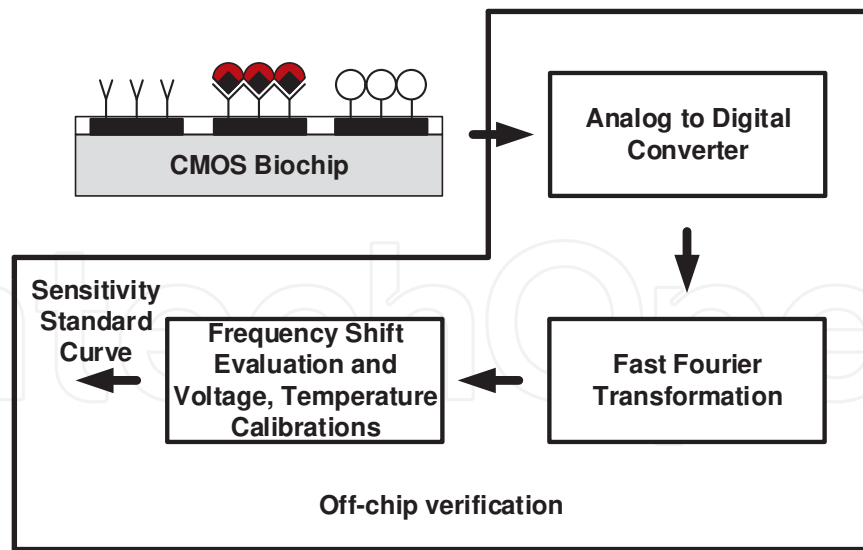


Figure 12. Simulated magnetic field uniformity on the optimized inductor surface.

#### 4.2.2. Biochip design

The block diagram of a CMOS high sensitivity oscillator-based biochip is shown in Figure 13. On different detection regions in a microarray, the output oscillation signal from the LC oscillators is firstly processed by a multiplexer for selection. It is then down-converted to an intermediate frequency (IF) and subsequently extracted by a low noise band-pass filter (BPF) for out-of-band noise and spur suppression. The frequency synthesizer and circuitry supply can be realized either on-chip or off-chip, depending on the applications. The IF signal is further



**Figure 14.** Block diagram of a CMOS high sensitivity oscillator-based biochip front-end and signal processing back-end.

digitized by an ADC off-chip, as shown in Figure 14. FFT is applied on the digitized IF signal to calculate the frequency shift induced by the attached MNPs and eventually, obtain the standard curve for biodetection and evaluation purposes. The ADC, FFT and following calculation can be verified through off-chip and commercial chips/FPGA/Matlab. It is then considered to be realized on-chip for a system-on-a-chip (SoC) solution.

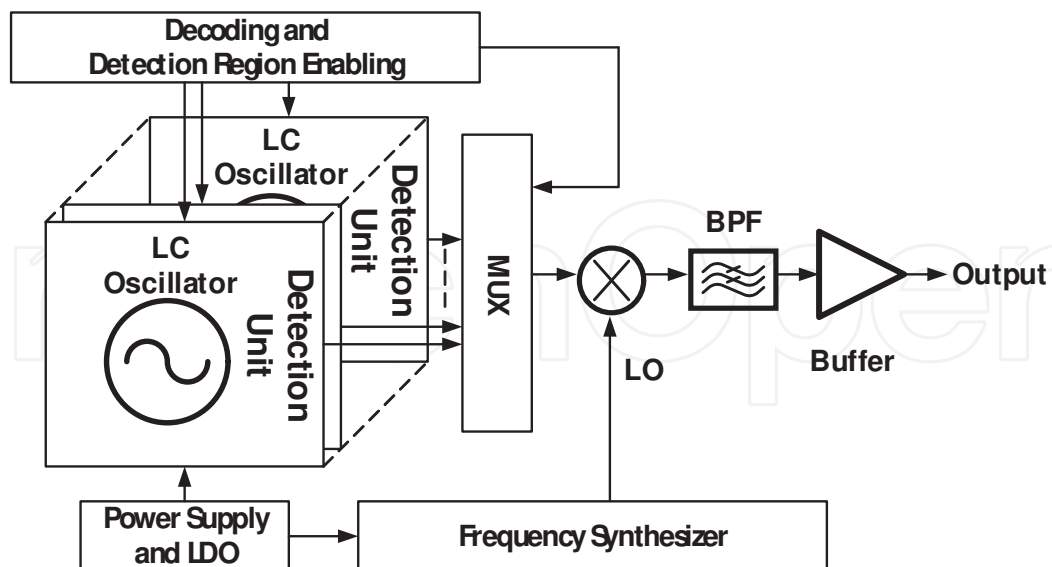


**Figure 13.** Circuit schematic of the oscillator-based biochip.

The challenging parts from the front-end biochip and back-end circuits are from the following aspects.

#### 4.2.2.1. Architecture of the signal down-conversion chain

The down-conversion chain of the proposed oscillator-based biochip is similar to that of the conventional RF front-end circuits for wireless communication, including direct conversion and heterodyne architectures. Since the output from a detection unit is a large signal with high output swing and considering the injection pulling effects, the LO signal from the frequency synthesizer should be at a different frequency from the unit. On the other hand, since the frequency of interest is around 1 GHz - 1.5 GHz, a double conversion is less efficient, owing to the power hungry dividers, buffers, etc. Therefore, a low IF architecture is preferred, considering the trade-off among architectures, complexity and power.

#### 4.2.2.2. Optimization of LO frequency

Being different from conventional receivers, there are no imaging effects in the proposed biochip. Unfortunately, the selection of LO should be traded with the dynamic range and sensitivity. A high LO would induce a reduction in the dynamic range and sensitivity, while an over-low LO frequency would increase the IF frequency, burdening the design of BPF and increasing power. The LO frequency has to be optimized based on the considerations of sensitivity, dynamic range and power.

As shown in Figure 14, FFT is applied on the digitized IF signal from the ADC in order to calculate the frequency shift induced by the attached MNPs and eventually, obtain the standard curve for biodetection and evaluation purposes.

In this part, we need to apply a Hanning window on the signal to suppress the spectrum leakage of FFT, before translating it into frequency domain. This improves the spectrum uniformity and sensitivity.

#### 4.2.3. Calibrations

Frequency drifting is a major issue for oscillator-based microarray biochips. Conventional assays introduce an additional LC tank for reference in order to cancel out the common-mode noises including drifts and PVT variations, however, increasing the chip area due to the large footprint of the on-chip inductor [24]. In this section, an "in-situ switched capacitor (ISSC) based calibration" scheme is presented by introducing only one switched capacitor in the LC tank for common-mode noise rejection, as shown in Figure 15. An enabling switch is used for the state switching and the measured frequencies between the adjacent time cycles are subtracted for the cancellation of common-mode voltage and temperature variations. The obtained frequency offsets in the initial state  $f_{offset}$  and after introducing the MNPs  $f'_{offset}$  follow that:

$$f'_{offset} = f_{offset} \left( 1 - \frac{\Delta L}{2L_0} \right) \quad (12)$$

Then, we have:

$$\frac{\Delta L}{2L_0} = 1 - \frac{f'_{offset}}{f_{offset}} = \frac{\Delta f}{f_0} = \frac{\alpha M}{2L_0} \quad (13)$$

Since all of the frequency drifting relating to the voltage and temperature variations are common-mode and cancelled out, the output signal, which is proportional to the MNP density within the inductor detection region, can therefore be obtained from the above relation.

The switching time has to be optimized, considering the typical voltage and temperature variation rates for the best cancellation. In this prototype, an empirical value of 0.1 s is found. In comparison to conventional dual-site cancellation scheme, this method is advantageous in terms of both circuit complexity and cost areas, supporting more detection regions on a single chip. It is capable of swiping out both drifts and PVT variation and does not require complicated external processing. Therefore, it improves the sensitivity and reliability of the multi-target detection, as well as simplifying the implementation.

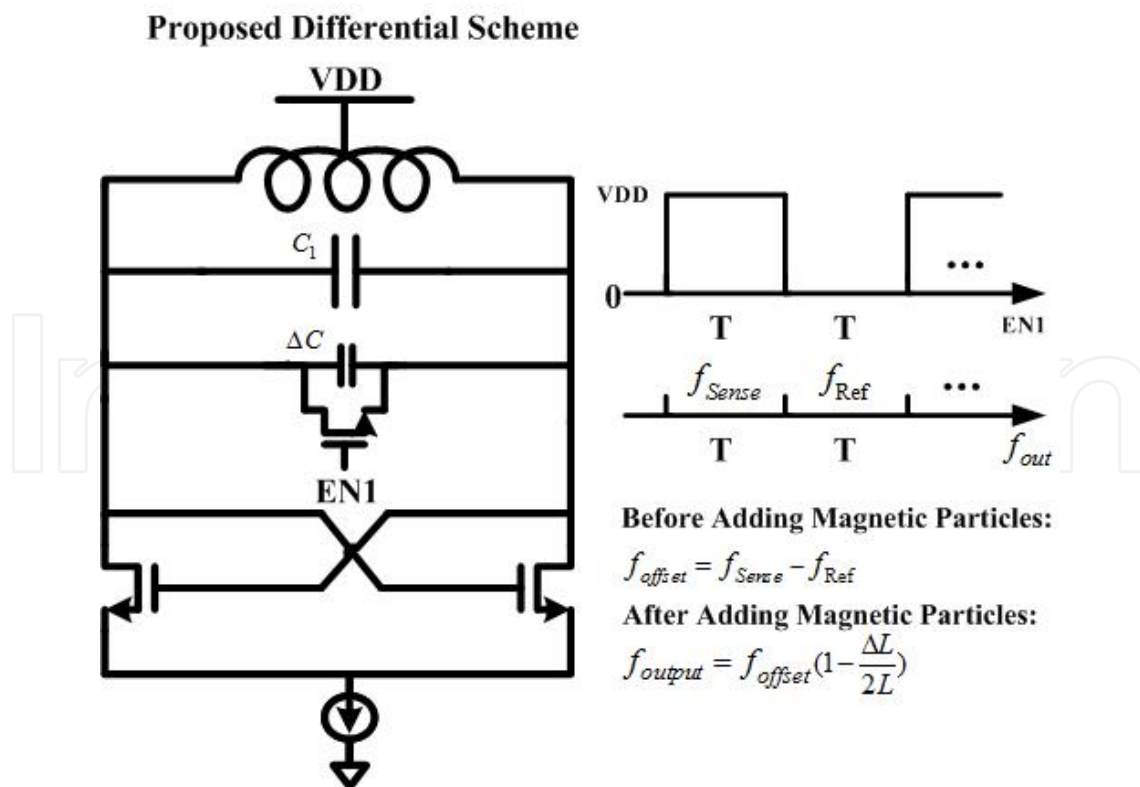
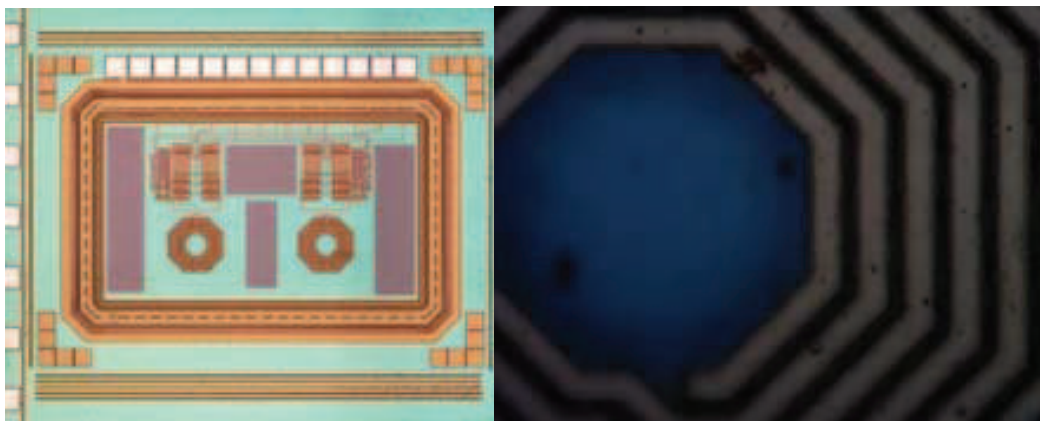


Figure 15. ISSC differential reference scheme for the voltage and temperature calibrations.

#### 4.2.4. Experimental results and discussions

An oscillator-based microarray biochip prototype has been designed and fabricated in the standard 180 nm CMOS process. The die micrograph is shown in Figure 16(a). The chip is designed with two inductor detection regions, which are 130  $\mu\text{m}$  in diameter. The measured results show that the oscillator works properly at a centre frequency of 1.45 GHz, with a phase noise of -120 dBc/Hz at 1 MHz offset and an output swing of larger than 1.25 V, while consuming 55 mW of power.

In the experiment, a standard 500 nm MNP sample solution has been utilized for verification and evaluation of the oscillator-based microarray biochip. The microscope picture of the distributed MNPs on the inductor detection region of the biochip is shown in Figure 16(b). The sample solution has been diluted by 50, 500, 5000 and 50000 times, respectively. The measured output frequency offset versus the dilution ratio is shown in Figure 17.



**Figure 16.** (a): Die micrograph of the oscillator-based microarray prototype and (b) the distributed MNPs on the inductor detection region of the oscillator-based microarray biochip.

It is found that the oscillator-based biochip works properly and a frequency shifting sensitivity of about 17 kHz has been achieved, roughly corresponding to about 10 ppm. The proposed ISSC calibration scheme is further applied and characterized through experiment. The output frequency shifts corresponding to different numbers of MNPs on the detection region are measured as shown in Figure 18, in which the exact quantity of MNPs is obtained from scanning electron microscope (SEM) images. The effective noise floor (defined as the standard deviation of measured frequency shift) of the sensor after ISSC calibration is 896 Hz, corresponding to about 0.62 ppm, and the extrapolated frequency shift for one single 500 nm MNP is 138.5 Hz which is related to the size and material of the MNPs, running frequency, and inductor structure. The maximal frequency shift is measured as 9.2 MHz, implying a dynamic range of at least 80.2 dB, while the area of the sensor detection region is only 60000  $\mu\text{m}^2$ , well below other calibration schemes. The comparisons with prior arts are shown in Table 2.

Compared with the electrochemical, GMR and MTJ biosensing strategies, the oscillator-based microarray biochip potentially features high sensitivity, good compatibility with CMOS technology, low cost, and multi-target capabilities.

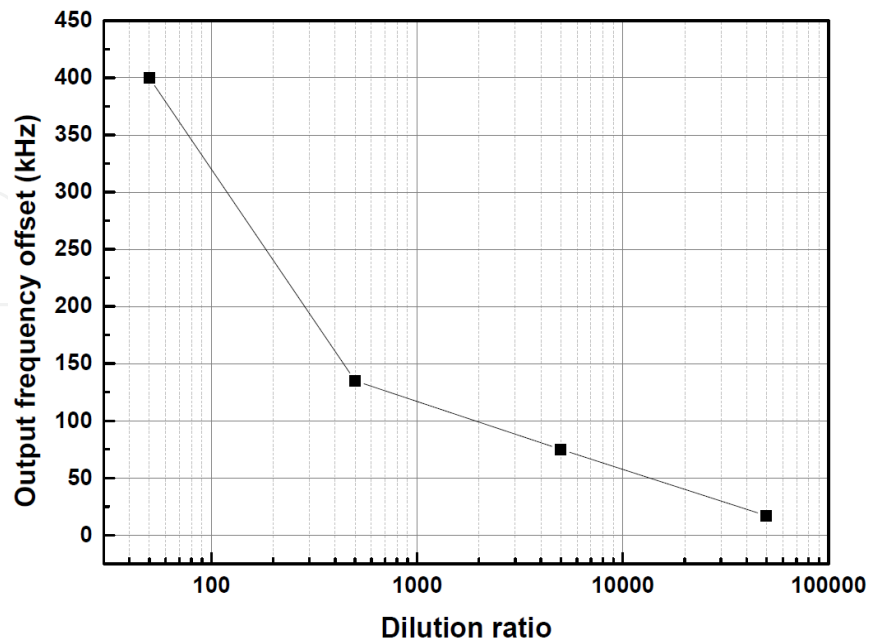


Figure 17. The measured output frequency offset versus the dilution ratio.

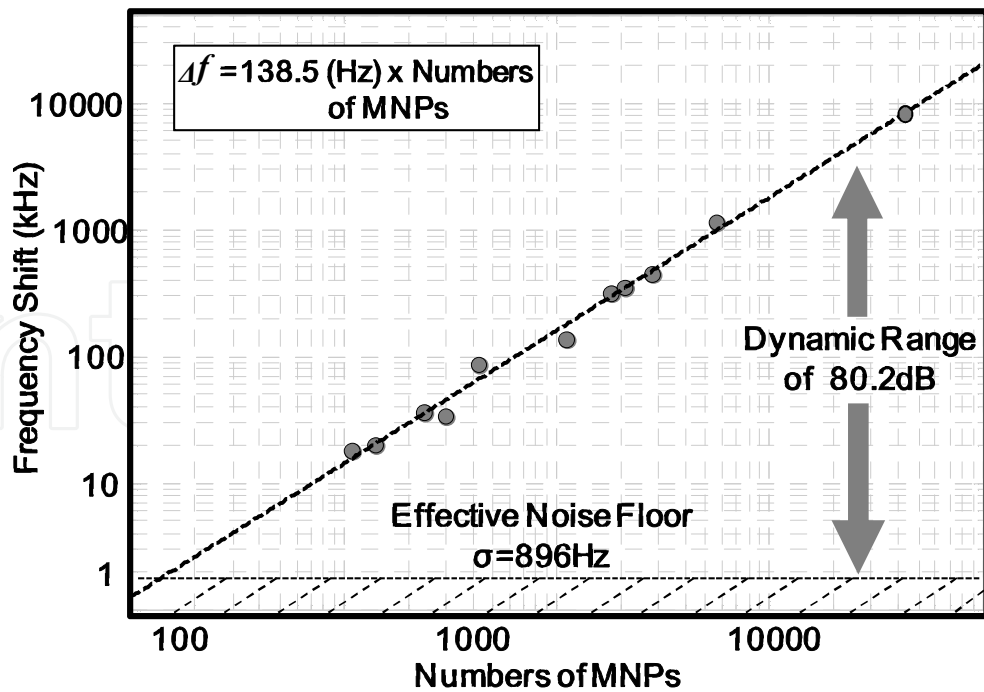


Figure 18. Frequency shifts corresponding to different numbers of MNPs.

	ISSC scheme This work	Differential scheme [17]	CDC scheme [17]
Operation freq. $f_0$	1.44 GHz	1.13 GHz	1.13 GHz
Phase noise at 1MHz	-123.4 dBc/Hz	-120.3 dBc/Hz	-120.3 dBc/Hz
Dynamic range	80.2 dB	85.4 dB	85.4 dB
Effective noise floor/ operation freq.	0.62 ppm	1.07 ppm	0.35 ppm
On-chip area per sensing region	60000 $\mu\text{m}^2$	>72000 $\mu\text{m}^2$	72000 $\mu\text{m}^2$
Technology	0.18- $\mu\text{m}$ CMOS	45-nm SOI CMOS	45-nm SOI CMOS

**Table 2.** Comparisons with state-of-the-art oscillator-based biochips with calibrations.

## 5. Conclusions and future directions of IMB

Silicon-based IMBs with high sensitivity and multi-target capabilities have caught the attention of both industry and academia for future accurate and early disease diagnosis and treatment. Compared with conventional assays, such as ELISA and fluorescent detections, CMOS IMBs are advantageous in various aspects. Such advantages include low cost, large-scale, readily integration with signal extraction and processing front-end and back-end circuits monolithically for a lab-on-a-chip solution, etc. In this chapter, state-of-the-art silicon-based IMB assays, including electrochemical microarray biochips, GMR and MTJ microarray biochips and fully CMOS compatible oscillator microarray biochips, are reviewed and discussed. Multiple challenges and issues, as well as novel techniques in the research and production of silicon-based IMB, are also presented.

In summary, silicon-based IMB provides fertile ground for future innovations. More specifically, electrochemical microarray biochips are one type of widely interested assay, which are capable of mid-sensitivity multi-target detection. In future research, various issues need to be solved such as background noise and random currents in a biochemical sample solution medium during the shrinking of electrode feature size, post-CMOS fabrication technologies and parallel back-end signal processing and mode recognition. MTJ and GMR microarrays assays are proved with extremely high sensitivities and provide full support to multi-target (~100 targets) biochemical analysis applications. However, both biochips require extra fabrication flow beyond the CMOS process, preventing the monolithic integration with acquisition IC front-end, signal processing back-end and DSP for a SoC solution in order to further improve system performance and reduce costs. Efforts have to be made to fix the process compatibility issues. This can be achieved through chip-level integration and system-in-a-package (SiP) solutions, etc. The oscillator-based microarray biochip features high sensitivity, wide dynamic range, multi-target capabilities and full compatibility with CMOS technology. Thus, it is potentially a suitable candidate for future SoC solutions. Calibration

techniques for phase noise of LC oscillators and frequency drifting due to PVT variations remains challenging and requires further innovations.

## Acknowledgements

The authors would like to thank the support of the National Natural Science Foundation of China under grant 61101001 and Tsinghua University Initiative Scientific Research Programme.

## Author details

Lei Zhang<sup>1\*</sup>, Cheng Zhu<sup>1</sup>, Jinwen Geng<sup>1</sup>, Xizeng Shi<sup>2</sup>, Yunhua Gao<sup>3</sup>, Zhijie Chang<sup>4</sup> and He Qian<sup>1</sup>

\*Address all correspondence to: [zhang.lei@tsinghua.edu.cn](mailto:zhang.lei@tsinghua.edu.cn).

1 Institute of Microelectronics, Tsinghua University, Beijing, China

2 Dongguan Bosh Biotechnologies, LTD., China

3 Technical Institute of Physics and Chemistry of the Chinese Academy of Sciences (CAS), China

4 Medical School, Tsinghua University, Beijing, China

## References

- [1] Cheng and L.J. Kricka. *Biochip Technology*. Harwood Academic Press; 2001.
- [2] P.A. Serra, editor. *Biosensors*. InTech; 2010.
- [3] T. G. Drummond, M. G. Hill, and J. K. Barton. Electrochemical DNA Sensors. *Nature Biotechnology*. 2003;21(10):1192-1199.
- [4] M. Schienle, A. Frey, F. Hofmann, B. Holzapfl, C. Paulus, P. Schindler-Bauer, R. Thewes. A Fully Electronic DNA Sensor with 128 Positions and In-Pixel A/D Conversion. In: *IEEE ISSCC Digest of Technical Papers*; February; 2004. p. 220-221.
- [5] M. Augustyniak, C. Paulus, R. Brederlow, N. Persike, G. Hartwich, D. Scmitt-Landsiedel, and R. Thewes. A 24×16 CMOS-Based Chronocoulometric DNA Microarray. In: *IEEE ISSCC Digest of Technical Papers*; February; 2006. p. 59-60.

- [6] B.C. Jang, P.Y. Cao, A. Chevalier, A. Ellington, and A. Hassibi. A CMOS Fluorescent-based Biosensor Microarray. In: IEEE ISSCC Digest of Technical Papers; February; 2009. p. 436-437.
- [7] L. Zhang, X.Q. He, Y. Wang, and Z.P. Yu. A Fully Integrated CMOS Nanoscale Biosensor Microarray. In: IEEE Custom Integrated Circuits Conference (CICC); September; 2011. p. 1-4.
- [8] R. Thewes, C. Paulusa, M. Schienlea, F. Hofmanna, A. Freya, P. Schindler-Bauera, M. Atzesbergera, B. Holzapfla, T. Hanedera, and H.-C. Hankea. A CMOS Medium Density DNA Microarray with Electronic Readout. In: Material Research Society Symposium; 2005. p. D3.4.1-D3.4.11.
- [9] J. Lian. A Fully Automated IVD System Based on MTJ arrays and Superparamagnetic Particles. *Journal of Applied Physics*. 2012;111(7):07B315.
- [10] D.A. Hall, R.S. Gaster, K.A.A. Makinwa, S.X. Wang, B. Murmann. A 256 Pixel Magnetoresistive Biosensor Microarray in 0.18 $\mu\text{m}$  CMOS. *IEEE Journal of Solid-State Circuits*. 2013;48(5):1290-1301.
- [11] C. Zhu, L. Zhang, X.Z. Shi, Y.H. Gao, Z.J. Chang, and H. Qian. A GMR Biosensing System with Sub-50ppm Sensitivity. In: IEEE International Conference on Electron Devices Solid-state Circuits (EDSSC); June; 2014.
- [12] W. Wang, Y. Wang, L. Tu, T. Klein, Y. Feng, J.P. Wang. Surface Modification for Protein and DNA Immobilization onto GMR Biosensor. *IEEE Transactions on Magnetics*. 2013;49(1):296-299.
- [13] H. Yang, B. Qu, B. Lei. Giant Magnetoresistive Biosensor for Myoglobin Immunoassay. In: IEEE Conference on Sensors; 2011. p. 805-808.
- [14] B.M. de Boer, J.A.H.M. Kahlman, T.P.G.H. Jansen, H. Duric, J. Veen. An Integrated and Sensitive Detection Platform for Magneto-Resistive Biosensors. *Biosensors and Bioelectronics*. 2007;22(9):2366-2370.
- [15] H. Wang, Y. Chen, A. Hassibi, A. Scherer, and A. Hajimiri. A Frequency-shift CMOS Magnetic Biosensor Array with Single-bead Sensitivity and No External Magnet. In: IEEE ISSCC Digest of Technical Papers; February; 2009. p. 438-439, 439a.
- [16] H. Wang. Magnetic Sensors for Diagnostic Medicine. *IEEE Microwave Magazine*. 2013;14(5):110-130.
- [17] H. Wang, C.-C. Weng, and A. Hajimiri. Phase noise and fundamental sensitivity of oscillator-based reactance sensors. *IEEE Transactions on Microwave Theory and Techniques*, 2013;61(5):2215-2229.
- [18] R.M. Lequin. Enzyme Immunoassay (EIA)/Enzyme-Linked Immunosorbent Assay (ELISA). *Clinical Chemistry*. 2005;51(12):2415-2418.

- [19] S. Weiss. Fluorescence Spectroscopy of Single Biomolecules. *Science*. 1999;283(5408): 1676-1683.
- [20] S. Ayers, K.D. Gillis, M. Lindau, and B.A. Minch. Design of a CMOS Potentiostat Circuit for Electrochemical Detector Arrays. *IEEE Transactions on Circuits and Systems I: Regular Papers*. 2007;54(4):736-744.
- [21] Basu, R.W. Robucci, and P.E. Hasler. A Low-power, Compact, Adaptive Logarithmic Transimpedance Amplifier Operating Over Seven Decades of Current. *IEEE Transactions on Circuits and Systems I: Regular Papers*. 2007;54(10):2167-2177.
- [22] L. Zhang, Z.P. Yu, and X.Q. He. Design and Implementation of Ultralow Current-Mode Amplifier for Biosensor Applications. *IEEE Transactions on Circuits and Systems II: Express Briefs*. 2009;56(7):540-544.
- [23] G. Ferrari, F. Gozzini, and M. Sampietro. A Current Sensitive Front-end Amplifier for Nano-Biosensors with a 2MHz BW. In: *IEEE ISSCC Digest of Technical Papers*; February; 2007. p. 164-165.
- [24] B. Razavi. *RF Microelectronics*. 2<sup>nd</sup> ed. Prentice Hall; 2012.
- [25] C. Brosseau and P. Talbot. Effective Magnetic Permeability of Ni and Co Micro- and Nanoparticles Embedded in a ZnO Matrix. *Journal of Applied Physics*. 2005;97(10): 104325-1-11.
- [26] Y. Zheng and J.G. Tront. Biological Agent Sensing Integrated Circuit (BASIC): A New CMOS Magnetic Biosensor System. In: *IEEE Sensors*; October; 2012. p. 1-4.

IntechOpen

